Linear eddy simulations of mixing in a homogeneous turbulent flow

Patrick A. McMurtry, Todd C. Gansauge, Alan R. Kerstein, and Steven K. Krueger

Citation: Physics of Fluids A: Fluid Dynamics **5**, 1023 (1993); doi: 10.1063/1.858667
View online: https://doi.org/10.1063/1.858667
View Table of Contents: http://aip.scitation.org/toc/pfa/5/4
Published by the American Institute of Physics

Linear eddy simulations of mixing in a homogeneous turbulent flow

Patrick A. McMurtry and Todd C. Gansauge
Department of Mechanical Engineering, University of Utah, Salt Lake City, Utah 84112

Alan R. Kerstein
Combustion Research Facility, Sandia National Laboratories, Livermore, California 94550

Steven K. Krueger
Department of Meteorology, University of Utah, Salt Lake City, Utah 84112

(Received 24 April 1992; accepted 24 November 1992)

The linear eddy mixing model is used to predict the evolution of a decaying scalar field in statistically steady homogeneous turbulent flow over a wide range of Reynolds and Schmidt numbers. Model results at low Reynolds number and order unity Schmidt number are shown to be in good overall agreement with direct numerical simulations. Results at higher Schmidt and Reynolds numbers reproduce conventional scaling properties of the scalar statistics. Predictions of Schmidt number and Reynolds number sensitivity of the evolution of the scalar concentration probability density function are presented and interpreted.

I. INTRODUCTION

The decay of a scalar field in a homogeneous turbulent flow has emerged as a standard test problem for models of mixing in turbulent flow fields. Two broad classes of models are commonly considered. The classical treatment of turbulent flows is based on a decomposition of the dependent variables into mean and fluctuating components (Reynolds decomposition). Solutions for the mean values are sought, with scalar transport modeled by assuming gradient diffusion. Turbulent transport is handled by introducing an *effective diffusivity* that is determined by flow field conditions. Other approaches are based on solving for the probability density function (pdf) of the scalar field. If the one-point pdf is known, moments and other one-point statistical information on the scalar field can be obtained. However, evolution equations for the single-point pdf require information on the joint statistics of the scalar and its dissipation rate. Several models have been developed in an attempt to describe the mixing process.[1,2] These models do not fully capture the underlying physical mechanisms, and none of them satisfactorily predict the scalar rms decay in a homogeneous turbulent flow field.[3]

The problems associated with modeling molecular mixing and chemical reaction can, in part, be traced to the difficulty of realistically describing and resolving the physical processes of turbulent convection (stirring) and molecular diffusion at the smallest scales of the flow—two distinctly different physical processes. Turbulent stirring is effective at redistributing the scalar field at all length scales above the Kolmogorov scale, while molecular diffusion acts most effectively at the smallest scalar length scales of the flow. An accurate description of mixing thus requires a realistic treatment of the flow at the smallest hydrodynamic and scalar length scales. Most mixing models involve an *ad hoc* treatment of the small-scale processes that include no distinction between turbulent stirring and molecular diffusion.

Investigations of mixing in homogeneous turbulence using direct numerical simulation have provided an extensive data set on the evolution of the scalar field statistics.[3,4] These studies have involved the use of a pseudospectral scheme to simulate the evolution of the scalar field on a 64^3 grid with periodic boundary conditions. Owing to the extreme range of length scales in turbulent reacting flows, resolution of all relevant length scales is computationally demanding. Complete resolution of the dynamic range of length and time scales was achieved by restricting the simulations to moderate-Reynolds number ($\mathrm{Re}_\lambda \approx 50$ or $\mathrm{Re}_l \approx 100$) and order unity Schmidt number, Sc. Since all relevant length scales were resolved and highly accurate numerical methods were employed, the statistics computed can be confidently treated as predictions of the scalar field behavior under the condition of moderate Re, homogeneous flow in a periodic domain.

Eswaran and Pope[4] investigated the evolution of the scalar field pdf and the effects of various initial scalar length scales on the scalar field statistics. Their initial scalar field consisted of blobs of scalar concentration of -1 and $+1$, with some smoothing to ensure that the scalar field was resolved numerically. The computational domain was a three-dimensional box, and the velocity field was numerically "forced" to maintain a statistically steady state. The initial velocity to scalar length scale ratio was shown to have a large effect on the initial rate of scalar rms decay, but the decay rate eventually became independent of the initial scalar length scale ratio. This observation differed from the experimental results of Warhaft and Lumley,[5] which showed a lasting dependence of the scalar rms decay on the initial scalar length scale. It was suggested by Eswaran and Pope that the difference between the experiments and simulation was a physical consequence of the adoption of a statistically steady velocity field in the simulation, in contrast to a decaying turbulence field in the experiments. This interpretation is supported by a recent DNS study of a similar configuration involving a decaying turbulence field.[6]

 0899-8213/93/041023-12$06.00

McMurtry and Givi[3] studied a configuration similar to Eswaran and Pope using direct simulation. The velocity field was forced at the lowest wave numbers, and the initial scalar field ϕ, consisted of two slabs: one with $\phi=1$ and the other with $\phi=-1$. In addition to pure mixing, they also investigated the evolution of the statistics of a reacting scalar. The primary objective of this work was to assess a number of mixing models[1,2,7] and study the effect of reaction on the scalar statistics. None of the models investigated predicted the correct behavior for the scalar pdf. It was shown that the reacting scalar did not tend toward a Gaussian distribution.

For a passive scalar, the question of the asymptotic form of the scalar pdf in steady, homogeneous turbulence has been addressed in a number of recent modeling studies, as well as in DNS studies. Using DNS, Eswaran and Pope found that the shape of the scalar pdf as it evolved in time was not sensitive to the initial length scale ratio, and it evolved from the initial bimodal form toward a Gaussian. Valiño and Dopazo[8] obtained a family of pdf's in good agreement with the DNS results, using a model that, by construction, yielded a Gaussian pdf in the limit of vanishing rms. Mapping closure[9] generates a family of pdf's that is also in good agreement with DNS,[10,11] yet the scalar statistics display persisting non-Gaussian behavior as the scalar rms vanishes.[11,12] Another model indicating non-Gaussian behavior has also been developed.[13]

Interpretation of these results is hindered by the narrow range of Re and Sc accessible by DNS and by the insensitivity of predicted families of pdf's to these parameters. (In the aforementioned models, these parameters influence the rate of evolution, but not the family of pdf's that is obtained.) A complete mechanistic description of turbulent mixing, with regard to pdf shape evolution or any other measurable property, should reflect the sensitivity of the mixing process to all the governing parameters. On this basis, it is evident that the analytical and computational methods employed to date have not provided a complete characterization of the mixing process.

In this paper, the linear eddy model, developed by Kerstein,[14,15] is used to study the evolution of a scalar field in a steady, homogeneous turbulent flow field over a wide range of Reynolds and Schmidt numbers. One of the features that distinguishes the linear eddy model from other more commonly used mixing models (e.g., eddy diffusivity, coalescence–dispersion models, mapping closure) is that all relevant length scales, even for relatively high-Re flows, are resolved. This is achieved by reducing the description of the scalar field to one spatial dimension. By resolving all length scales, the mechanisms of turbulent convection and molecular diffusion can be treated distinctly, even at the smallest diffusion scales. Parametric sensitivities can therefore be addressed on the basis of the underlying physical mechanisms.

In previous work, the linear eddy model has been applied to mixing in spatially developing flows and to a homogeneous, statistically steady mixing configuration. These applications served both to validate aspects of the model and to provide mechanistic interpretations of measured properties in a unifying framework.

A statistically steady configuration can be obtained by imposing a uniform scalar gradient on a homogeneous turbulent flow field, resulting in relaxation of the mean scalar rms to a constant nonzero value after a transient interval. Computations for this configuration reproduced key features of the scalar power spectrum, including dependences of Reynolds and Schmidt numbers, and scaling properties of higher-order scalar statistics, thus validating the model representation of micromixing kinematics.[15]

The applications to spatially developing flows collectively demonstrate that the diverse phenomenology observed in such flows may be viewed as various manifestations of a simple underlying kinematic picture. In such applications, configuration-specific aspects are reflected in the initial and boundary conditions of the computations and in the model analogs of quantities, such as Re, Sc, and Da (Damköhler number), but the underlying kinematic picture is the same in all cases. On this basis, the model reproduces the following measured properties: (1) three distinct scaling regimes governing turbulent plume growth, and spatially resolved scalar fluctuation statistics within such plumes;[14,16] (2) the spatially resolved cross-correlation of diffusive scalars in a three-stream mixing configuration;[16] (3) Da dependences of reactant concentrations in a two-stream configuration;[16] (4) spatially resolved scalar fluctuation statistics in free shear flows, and the dependence of local and overall shear-flow mixing on Re and Sc,[17–19] and (5) scalar fluctuation statistics reflecting differential molecular diffusion effects.[18] The unification of this diverse phenomenology achieved by linear eddy modeling is unprecedented.

A category of mixing configurations to which the model has not previously been applied is spatially homogeneous, transient mixing. Spatial homogeneity facilitates the interpretation of results in terms of simple scaling ideas, while transient effects introduce some of the phenomenological richness of spatially developing flows. It is largely for these reasons that the DNS study of such a configuration by Eswaran and Pope[4] has come to be regarded as a paradigm of the turbulent mixing problem, and has motivated many subsequent numerical and analytical studies.

The objectives of the present study are twofold. First, linear eddy computations, based on a formulation that incorporates high-Re inertial-range scalings, are compared to the results of Eswaran and Pope in order to demonstrate the applicability of such a picture to their moderate-Re results. Second, computations are performed beyond the limited range of Re and Sc accessible by DNS in order to extrapolate the DNS results to other regimes of physical interest. Re and Sc dependences of computed quantities are found to be consistent with simple scalings, based on dimensional considerations, where such considerations are applicable. Novel qualitative features of the evolution of the concentration probability density function (pdf) for high Sc are identified. Higher moments of the concentration field are found to relax to values that exhibit Sc- and

Re-dependent deviations from Gaussian values. These features, which are shown to be intuitively reasonable, constitute experimentally testable predictions.

II. LINEAR EDDY MODEL

The development of the linear eddy model has been described in detail elsewhere,[14,15] and is only briefly outlined here. This approach has a number of unique features that distinguish it from other more commonly used mixing models (e.g., eddy diffusivity and coalescence–dispersion models). In particular, the distinction between molecular diffusion and turbulent convection is retained at *all* scales of the flow in a computationally affordable simulation by reducing the description of the scalar field to one spatial dimension. Diffusion and convection have very different effects on scalar field evolution; accounting for these differences is crucial to accurately describe the species field, especially when chemical reactions are involved. This distinction has not been achieved by any previously proposed mixing model.

Velocity field statistics are inputs into the model, although no explicit velocity field appears. The required model parameters that describe the flow field include the turbulent diffusivity (D_T), the integral length scale (L), the Reynolds number, Re (which determines the Kolmogorov scale, η), and the Péclet number, Pe. Thus, the flow field properties are inputs to the linear eddy model, not predictions of the model. The formulation of the model presented here is reparametrized in terms of L, Re, and τ_L, where τ_L is the large eddy turnover time in the model and is defined as $\tau_L \equiv L^2/D_T$.

Reflecting the considerations above, the model involves two distinct mechanisms implemented concurrently, reflecting the distinct influences of molecular diffusion and turbulent stirring. The first mechanism acting on the scalar field, molecular diffusion, is straightforwardly implemented by numerical solution of the diffusion equation, $\partial\phi/\partial t = (1/\mathrm{Pe})(\partial^2\phi/\partial x^2)$, over the linear domain. Spatial resolution of the discretized linear domain is chosen (as elaborated in Sec. III B) so that grid effects are insignificant, i.e., the scalar fluctuation lengths are fully resolved.

The key feature of the model is the manner in which turbulent convection is treated. This is implemented by random rearrangements of the scalar field along a line. The frequency of these rearrangements is determined by requiring that the stochastic rearrangement events result in a turbulent diffusivity consistent with accepted scalings for high-Re turbulent flows. Each rearrangement event involves spatial redistribution of the species field within a randomly selected spatial domain. The size of the selected domain, representing the eddy size, is sampled from a distribution of eddy sizes that is obtained by applying Kolmogorov scaling laws. In this model, the spatial redistribution of a segment of length l represents the action of an eddy of size l. A rearrangement event is illustrated and described in Fig. 1.

The rearrangement process is governed by two parameters: λ, which is a rate parameter with dimensions ($L^{-1}t^{-1}$), and $f(l)$, a pdf describing the segment length

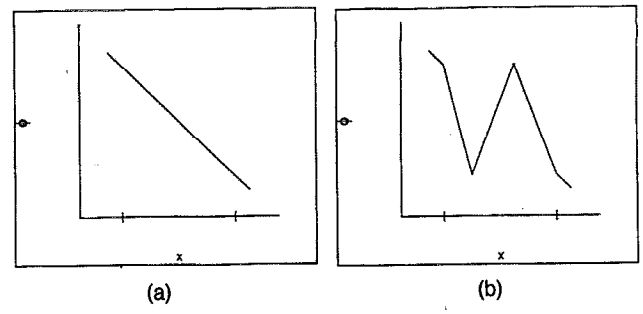

FIG. 1. The scalar rearrangement (turbulent stirring) process is carried out by the use of the "triplet" map. The triplet map involves selecting a segment of the linear domain for rearrangement, making three compressed copies of the scalar field in that segment, replacing the original field by the three copies, and inverting the center copy. (a) Initial scalar field, chosen in this illustration to be a linear function of spatial location. (b) Scalar field after rearrangement.

distribution. These parameters are determined by recognizing that the rearrangement events induce a random walk of a marker particle on the linear domain. Equating the diffusivity of the random process with scalings for the turbulent diffusivity provides the necessary relationships to determine λ and $f(l)$. For a high-Re turbulent flow described by a Kolmogorov cascade, the result of Kerstein[15] can be expressed as

$$f(l) = \begin{cases} \dfrac{5}{3}\dfrac{l^{-8/3}}{\eta^{-5/3} - L^{-5/3}}, & \eta \leqslant l \leqslant L, \\ 0, \quad \text{otherwise}, \end{cases} \tag{1}$$

$$\lambda = \frac{54}{5}\frac{1}{L\tau_L}\left(\frac{L}{\eta}\right)^{5/3}, \tag{2}$$

where the model turnover time τ_L is related to a particular empirically defined turnover time τ_{l_0} by a constant factor, $\tau_L = c\tau_{l_0}$ (see Sec. III C). Equation (1) defines model Kolmogorov and integral scales η and L, respectively, that bound the range of segment lengths.

Given an initial scalar distribution, the evolution of the scalar field is governed by the molecular diffusion process, punctuated by the random rearrangement events parametrized by $f(l)$ and λ. This formulation provides an approximate, yet physically sound, description of turbulent mixing. Namely, molecular diffusion is accounted for explicitly by numerical solution of the diffusion equation, while turbulent stirring (convection) is modeled by the stochastic scalar rearrangement events. By limiting application to one dimension, all relevant length and time scales can be resolved.

The scalar information within the linear eddy domain provides a statistical description of the scalar field. The one-dimensional representation of the three-dimensional scalar field can be interpreted as a space curve aligned with the local scalar gradient.[15] This interpretation is not unique, and it can be instructive in other cases to view the linear eddy domain as a particular spatial coordinate in the flow field.[16]

Having thus formulated the model, some of the features that render it a valid representation of multidimensional turbulent mixing are noted.

First, the mathematical formulation of the model involves a one-dimensional spatial domain that is, in principle, a continuum. In other words, there is no intrinsic limit on the spatial resolution. As in multidimensional flow simulations, a practical limit on spatial resolution is computational affordability. This consideration highlights a key advantage of the linear-eddy approach. Due to the restriction of the model to one spatial dimension, it is affordable to achieve sufficient resolution, so that an accurate approximation to the continuum formulation is obtained in simulations for Re values of practical interest.

This observation leads to the second feature, namely, the manner in which the physically correct microstructure of the scalar mixing field arises as a consequence of the continuum formulation of the model. This feature is discussed in detail elsewhere,[15] so the discussion here is limited to a few pertinent remarks. The continuum formulation has no predetermined intrinsic resolution, so the finest scale of the scalar field fluctuation is determined by the ongoing interaction of the two processes, molecular diffusion and random rearrangements, that are implemented concurrently during a linear eddy simulation.

Molecular diffusion is implemented deterministically using a finite difference scheme with sufficient time resolution to approximate the continuous-time limit. This ongoing smoothing process is randomly punctuated by instantaneous rearrangement events illustrated in Fig. 1, and parametrized by Eqs. (1) and (2). Each event causes a multiplicative increase in the scalar gradient within the selected segment, analogous to the effect of the compressive strain associated with a turbulent eddy of comparable size. The parametrization of event frequency as a function of segment size is formulated so that the frequency-versus-size relation governing the Kolmogorov eddy cascade is, in effect, built into the model.

Since the frequency-versus-size relation implies a characteristic time associated with each size, the question arises as to whether that characteristic time can be interpreted as the turnover time for eddies of that size. In the model, this is not literally the case, since individual rearrangement events are instantaneous. It is nevertheless plausible, though not guaranteed, that this interpretation is valid for the purpose of analyzing scaling properties of the model in the manner of Kolmogorov dimensional analysis. Scaling analysis of this sort, supported by numerical results of linear eddy simulations, verifies that most of the well-known phenomenology of turbulent mixing fields (spectral scaling exponents, wave-number ranges of the various scaling regimes, etc.) is captured by the model.[15] Additional verification is provided by computed results presented in Sec. IV.

In particular, the length scale at which diffusive and convective (i.e., rearrangement) effects balance is found to be the Batchelor scale, as defined in terms of its usual dependences on Re and Sc. Thus, to achieve sufficient spatial and temporal resolution for given Re and Sc, it is necessary to discretize the linear eddy domain into computational elements smaller than the Batchelor length scale (or smaller than the Kolmogorov scale if the latter scale is smaller, i.e., if $\mathrm{Sc} < 1$).

A third and final feature is noted. The triplet map illustrated in Fig. 1 is formulated so as to avoid causing discontinuities in the scalar field, although discontinuous derivatives are introduced. The latter artifact is a seemingly unavoidable consequence of the one-dimensional formulation. The only apparent impact of this artifact is a somewhat slow falloff of the scalar fluctuation intensity in the dissipation range (high-wave-number limit) of the scalar power spectrum.[15]

The upshot of these observations is that the linear-eddy model, though not entirely free of artifacts, has been found to provide a remarkably accurate overall representation of turbulent mixing phenomenology, despite the substantial simplifications necessitated by a one-dimensional representation.

III. APPLICATION TO SCALAR MIXING IN A HOMOGENEOUS TURBULENT FLOW

A. Scalar field initialization

The linear eddy model is applied here to mixing of a scalar field, ϕ, in a homogeneous turbulent flow field. (The analogous physical configuration is a three-dimensional flow field with periodic boundary conditions in a box of size B in each spatial dimension.) Within this domain the scalar field is initially distributed in blobs of concentration -1 and 1, with smooth transition layers at the interfaces. The transition layers are necessary to satisfy numerical resolution requirements in direct numerical simulations. The numerical specification of this scalar field for a three-dimensional DNS study is described by Eswaran and Pope.[4] In particular, the initial length scale of the scalar field is generated in a manner such that the initial scalar-energy spectrum is equal to a specified function, $f_\theta(k)$, where $f_\theta(k)$ is a top-hat function of width k_0, centered on a selected integer wave number k_s (k_0 is the smallest nonzero wave number resolved in the simulation). The ratio k_s/k_0 thus determines the integral length scale of the scalar field, ϕ. In the linear eddy model results presented here, the one-dimensional analog of this initialization is applied to a linear domain of $B=2\pi$. Note that the initialization procedure of Eswaran and Pope produces maximum and minimum values of ϕ outside the interval -1, $+1$. This is reflected in some of the pdf plots presented in Sec. IV. This artifact of the initialization does not, in any way, affect the integrity of the calculations.

For comparison with the results of Eswaran and Pope, various initial scalar fields with different scalar length scales were constructed by varying the ratio k_s/k_0. All additional parameters of the initialization are as specified by Eswaran and Pope. The one-dimensional implementation of their initialization procedure generates nonrandom scalar fields, but they are soon randomized by the spatial rearrangement events (eddy action). Figure 2 illustrates two

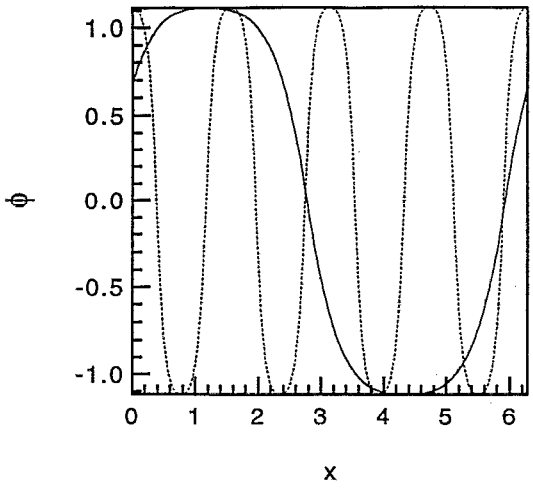

FIG. 2. Typical realizations of the initial scalar field on the linear domain $[0,2\pi]$. (—, $k_s/k_0=1$; ---, $k_s/k_0=4$).

of the different initial one-dimensional scalar fields that were used in this modeling study.

B. Algorithm and Implementation

The total number of computational elements along the domain must be chosen to resolve the largest and smallest scales in the flow. The computational domain was selected to include one integral scale, i.e., $B=L$. From Kolmogorov scalings, the ratio of the largest to smallest length scales in the flow is approximately $L/\eta=\mathrm{Re}^{3/4}$. For $\mathrm{Re}=10^4$, this ratio is 1000. By taking six computational elements to resolve the eddies at the Kolmogorov scale (i.e., $n_\eta=6$), 6000 elements are needed to resolve the complete flow field for $\mathrm{Re}=10^4$. Scalar field resolution requirements can be more stringent. The Batchelor scale, l_B, which must be resolved, is smaller than the Kolmogorov scale in high-Sc flows. Scaling arguments yield $\eta/l_B\sim\mathrm{Sc}^{1/2}$. A numerical sensitivity analysis indicated that approximately twice this number of grid points ($2\,\mathrm{Sc}^{1/2}\times n_\eta$) is needed per Kolmogorov scale before multipoint statistics (e.g., scalar dissipation) become insensitive to resolution.

The molecular diffusion process is implemented by regularly advancing the one-dimensional diffusion equation using a space-centered finite difference technique. To implement each rearrangement event, a location is randomly selected within the domain. The segment size is also randomly chosen, but in such a way as to satisfy the probability distribution given by $f(l)$. One rearrangement takes place per time interval $1/\lambda B$. The process is repeated until a desired time has elapsed.

The complete model is implemented as a Monte Carlo simulation of many individual flow field realizations. The statistics are then computed by averaging the ensemble of realizations. For each of the simulations presented below, the scalar field statistics were averaged over 1000 separate realizations (except the $\mathrm{Re}_S=10\,000$ case, in which 300 realizations were taken), yielding sufficient statistical precision for quantitative comparison to DNS results. Computed pdf's are generated using 100 bins over the scalar range of scalar values.

C. Model parameters

The early applications of the linear eddy model involved no parameter adjustments. The model is built upon scaling laws for high Re flows, and order unity coefficients implicit in the scale relationships were set equal to unity. Here, parameter assignments are based on the selected DNS comparison case in order to obtain direct quantitative comparisons. In particular, the model analogs of Sc, Re, and L must be related to their physical (DNS) counterparts.

The large-scale Reynolds number in the DNS of Eswaren and Pope was calculated to be $\mathrm{Re}_{l_0}\equiv u' l_0/\nu = 107$. The linear eddy analog of Re_{l_0} is $\mathrm{Re}_S\equiv(L/\eta)^{4/3}$, where L is the integral scale of the model. Based on this definition, the model Reynolds number Re_S was selected to give approximately the same range of eddy sizes as in the DNS. This was achieved as follows: The DNS used here to compare model results contained a wave number ratio of $k_{\max}/k_0=30$, where $k_{\max}$ and k_0 are the largest and smallest nonzero wave numbers in the simulation. Applying an eddy-size–wave-number analogy[20] yields an equivalent length scale ratio, $L/\eta=(2\pi/k_0)/(2\pi/k_{\max})=k_{\max}/k_0=30$, resulting in a model Reynolds number $\mathrm{Re}_S\approx 90$. The Schmidt number of the model Sc_S is taken to be $\mathrm{Sc}_S=0.7$, equal to the physical Schmidt number.

The final consideration is the relationship between the integral scale defined in the model, L and the measured integral scale in the DNS, l_0. The two are not equivalent since L is defined as the largest allowable eddy for a given flow, while l_0 represents a "typical" eddy size. As pointed out by Kerstein,[16] the relationship between L and l_0 is not universal since the definition of l_0 for different flows is not always consistent. The value of L in the model is taken as the domain size, $L=2\pi$. The data of Eswaran and Pope yield $l_0=1.01$, giving $L=6.22 l_0$. This is close to the value of $L=5.6 l_0$ found by Kerstein[16] in simulating the concentration field downstream of a line source in decaying homogeneous turbulence. With these model parameters determined, all computed statistical properties of the scalar field are predictions that can be compared directly with the simulation results.

To perform direct quantitative comparisons, the large eddy turnover time of the linear eddy model $\tau_L\equiv L^2/D_T$, must be related to the large eddy turnover time in the DNS, $\tau_{l_0}\equiv l_0/u'$. This was done by inferring the relationship between τ_{l_0} and D_T from the data reported in Eswaran and Pope. The chosen linear eddy model parameters imply a turbulent diffusivity based on the model definition $D_T/D_M=\mathrm{Re}_S\,\mathrm{Sc}_S=63$. The given molecular diffusivity used in the DNS ($D_M=0.035$) then implies a turbulent diffusivity $D_T=2.205$. From the reported values of u' and l_0 by Eswaran and Pope, a relationship for the turbulent diffusivity of the DNS can be expressed as $D_T=0.82u'l_0$. The time scale ratio between the linear eddy model and the DNS for the runs reported in the following is thus

$\tau_L/\tau_{l_0} = L^2/(0.82l_0^2) \approx 47$. In all model/DNS comparisons reported in Sec. IV A the time axis is scaled by τ_{l_0}. For the Schmidt and Reynolds number effects reported in Sec. IV B, time is scaled by the linear eddy turnover time, τ_L.

In addition to the comparisons presented in Sec. IV on the basis of the foregoing parameter assignments, additional comparisons have been performed in which different combinations of input parameters were varied by a factor of 2 or more. The quality of the agreement with simulation results was found to be only mildly sensitive to input parameter values, so the inferences drawn in Sec. IV are not strongly dependent on the mechanistic basis of the parameter assignments.

With regard to direct quantitative comparisons, it is noted that the parameters defining the linear eddy model [see Eqs. (1) and (2)] are developed based on Kolmogorov inertial range scalings, while the direct simulations that have been performed of scalar mixing to date display only a barely perceptible inertial range. As a result, the distribution of eddy sizes and frequencies in the linear eddy model and in the direct simulations cannot be made to match exactly. This can contribute to differences between model results and DNS data. Furthermore, it is expected that there will be some inherent limitations when describing the full three-dimensional turbulent mixing process in one dimension. However, previous results and the comparisons that follow demonstrate the ability of the linear eddy model to realistically represent the turbulent mixing process.

IV. MODEL RESULTS

Results of the linear eddy model model study are first directly compared to moderate-Re DNS. The model is then applied to study the mixing characteristics over a wide range of Reynolds and Schmidt numbers.

A. Comparison with direct numerical simulation

The decay of the scalar rms ϕ' for various initial scalar length scales is compared to DNS results in Fig. 3. The overall agreement is good, with better agreement seen in the cases with the larger initial scalar length scale. A discussion of the quantitative differences between the DNS and linear eddy results for the smaller initial scalar length scales is provided at the end of this section.

Both linear eddy and DNS indicate that in the final state of scalar rms decay, the decay rate becomes independent of the initial scalar length scale. It was suggested by Eswaran and Pope, and shown numerically by Mell *et al.*,[6] that this independence of the initial scalar length scale is a characteristic of scalar decay in a statistically steady turbulent flow. In decaying turbulence this is not observed.

Another, more subtle qualitative feature of the scalar rms decay curves is also captured by the linear eddy model. Note that for the case $k_s/k_0=1$ the rms decay curve is concave prior to the linear region. For higher values of k_s/k_0, the concave region is followed by a convex region before the linear region. This behavior has been described in detail by Kosály[21] and reflects his conjecture that in

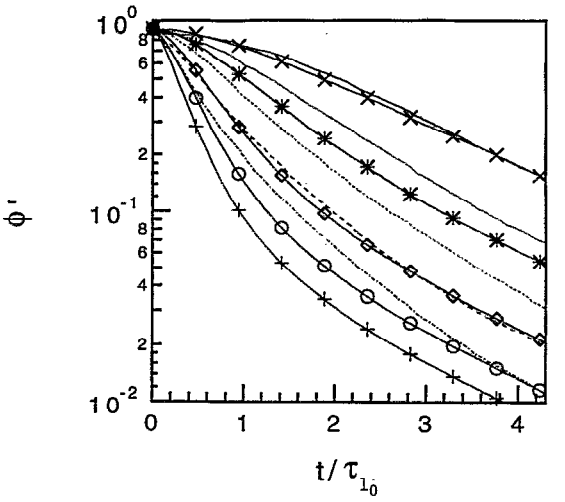

FIG. 3. Time evolution of the scalar rms ϕ' for simulations at $Re_S=90$ and $Sc_S=0.7$, compared with DNS of Eswaran and Pope (—, linear eddy simulation results) (×, $k_s/k_0=1$), (*, $k_s/k_0=2$), (◇, $k_s/k_0=4$), (○, $k_s/k_0=6$), (+, $k_s/k_0=8$). Eswaran and Pope results (solid line, $k_s/k_0=1$), (dots, $k_s/k_0=2$), (dashes, $k_s/k_0=4$), (long dash, $k_s/k_0=6$), (dot–dash, $k_s/k_0=8$) Time is normalized by $\tau_{l_0} = l_0/u'$.

stationary turbulence the scalar/velocity length scale ratio (l_θ/l) evolves to a value of unity, independent of initial length scale ratio. It has been shown by Kosály that the concave-linear shape of the rms decay curve corresponds to $l_\theta(t=0)/l \geqslant 1$ and the concave–convex–linear shape corresponds to $l_\theta(t=0)/l < 1$. In the former case, the scalar length scale decreases with time until $l_\theta(t)/l$ reaches its asymptotic values, while in the later case the ratio increases. This provides additional evidence that the physics governing the scalar length scale evolution is realistically represented by the linear eddy modeling process.

Based on the interpretation of the linear eddy computational domain as a space curve aligned with the scalar gradient, the model analog of the mean scalar dissipation, defined by Eswaran and Pope as $\langle \epsilon_\phi \rangle \equiv D_M \langle \nabla\phi \cdot \nabla\phi \rangle$, is $D_M \langle (\partial\phi/\partial x)^2 \rangle$. This quantity is computed by first differencing the discretized one-dimensional scalar field. The evolution of the mean scalar dissipation is shown in Fig. 4. The agreement with the DNS data is again good.

The largest discrepancy is seen to occur at early times, where the dissipation computed by the linear eddy model consistently grows at a faster rate than in the DNS. At later times the dissipation decays at a rate that is approximately independent of the initial scalar length scale.

The evolution of the concentration pdf for $k_s/k_0=1$ is shown in Fig. 5(a). At $t=0$ the initial field is approximately represented by a double delta distribution, indicating the initially unmixed scalar field. As time proceeds, turbulent mixing and molecular diffusion yield a mixed fluid concentration peaking at $\phi=0$. Figure 5(b) shows the development of the pdf, as predicted by the DNS of Eswaran and Pope for the same value of k_s/k_0. The family of pdf's evolving from the double delta function distribution to the final peak at the mixed fluid concentration is well

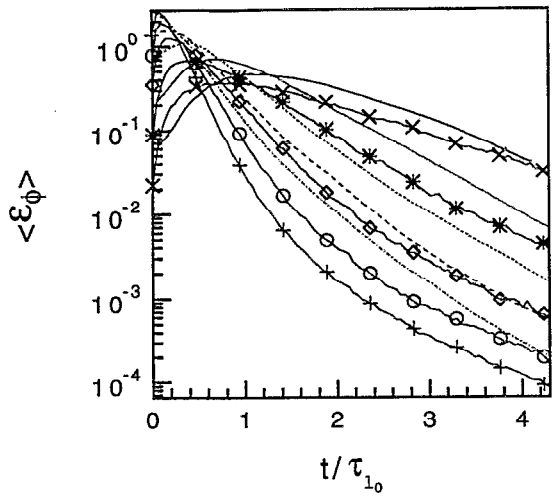

FIG. 4. Evolution of the mean scalar dissipation rate for same cases as Fig. 3.

represented by the linear eddy model. In particular, the transition from a bimodal to unimodal form is found to involve an intermediate form (at $\phi'/\phi_0' \approx 0.6$) with a broad plateau, as in the DNS results.

The evolution of the concentration pdf for $k_s/k_0=4$ is shown in Fig. 5(c). For this initialization the pdf displays some qualitative differences during its evolution from the case of $k_s/k_0=1$. Namely, there is an indication of trimodality during intermediate stages of the evolution. Some differences in the pdf evolution for different values of k_s/k_0 are also apparent in the higher-order moments (Figs. 6 and 7), as will be discussed shortly. This behavior was not observed by Eswaran and Pope, who found little dependence of the pdf evolution on k_s/k_0.

Trimodal pdf's indicate intermittency in the scalar field in the following sense. Sharp scalar interfaces are subject to rapid stirring by small eddies acting on relatively short time scales. (Recall from Sec. II that the model emulates the eddy-size-versus-time-scale relationship obeyed by inertial-range eddies.) This results in completion of local mixing near interfaces (and hence development of the central peak of the pdf) before large-scale mixing depletes the initial unmixed peaks. It is evident that the degree of sensitivity indicated by the linear eddy results is not supported by DNS. Nevertheless, the mechanistic plausibility of the trend suggests that a wider-ranging DNS parameter study to check the qualitative prediction would be worthwhile.

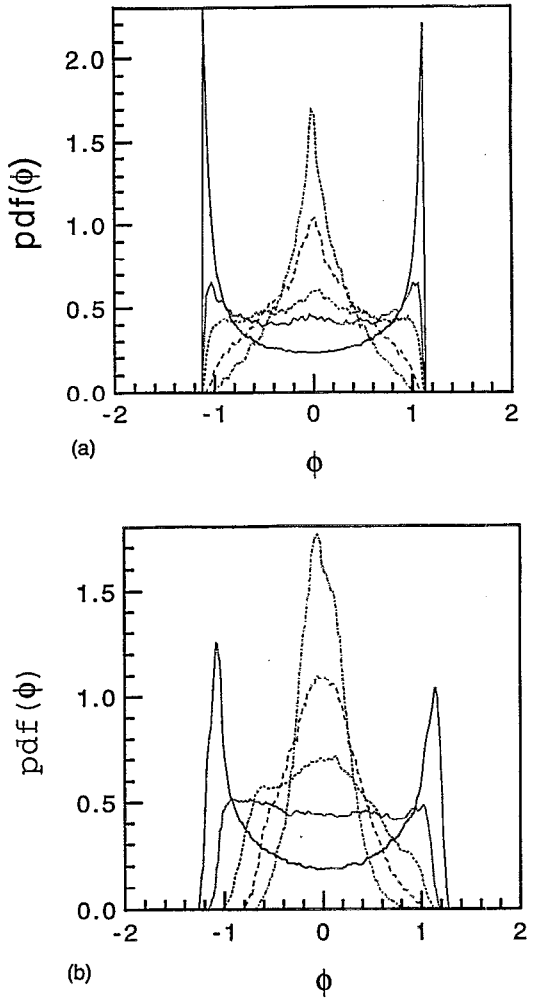

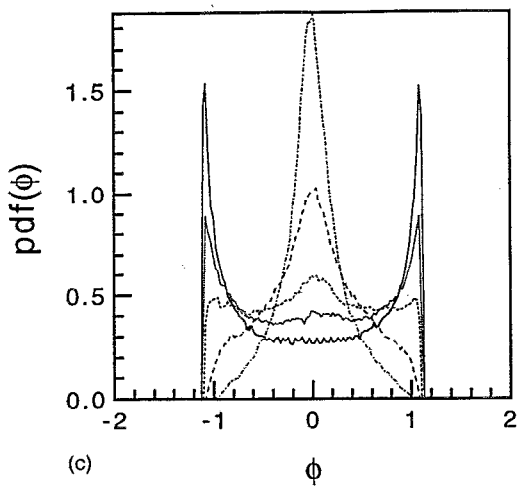

FIG. 5. Computed scalar pdf from (a) the linear eddy model for $Re_S=90$ and $Sc_S=0.7$, $k_s/k_0=1$. (Solid line, $\phi'/\phi_0' = 0.89$), (dots, $\phi'/\phi_0' = 0.72$), (dash, $\phi'/\phi_0' = 0.63$), (long dash, $\phi'/\phi_0' = 0.47$), (dot–dash, $\phi'/\phi_0' = 0.34$); and (b) DNS of Eswaran and Pope for $k_s/k_0=1$; (solid line, $\phi'/\phi_0' = 0.99$), (dots, $\phi'/\phi_0' = 0.73$), (short dash, $\phi'/\phi_0' = 0.55$), (long dash, $\phi'/\phi_0' = 0.40$), (dot–dash, $\phi'/\phi_0' = 0.27$). (c) Linear eddy model for the same case as (a), except $k_s/k_0=4$. (Solid line, $\phi'/\phi_0' = 0.93$), (dots, $\phi'/\phi_0' = 0.78$), (dash, $\phi'/\phi_0' = 0.70$), (long dash, $\phi'/\phi_0' = 0.63$), (dot–dash, $\phi'/\phi_0' = 0.40$).

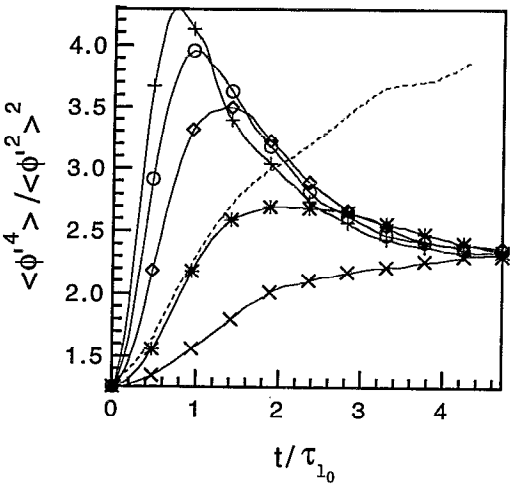

FIG. 6. Evolution of the kurtosis (normalized fourth moment) from the linear eddy model for $Re_S=90$, $Sc_S=0.7$. ($\times$, $k_s/k_0=1$), ($*$, $k_s/k_0=2$), ($\diamond$, $k_s/k_0=4$), ($\circ$, $k_s/k_0=6$), and ($+$, $k_s/k_0=8$). Eswaran and Pope DNS results for $k_s/k_0=4$ are indicated by a dashed line.

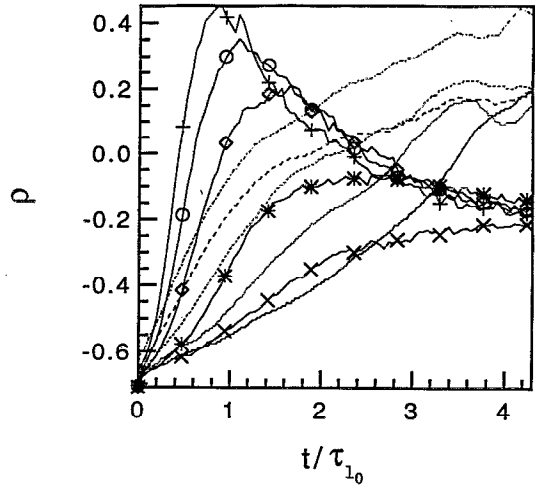

FIG. 8. Evolution of the scalar variance dissipation correlation function for the same cases as Fig. 3.

Related considerations bearing on the Sc sensitivity of pdf evolution are discussed in Sec. IV.

To analyze the structure of the pdf in more detail, it is instructive to examine some of the higher-order moments of the concentration field. In Figs. 6 and 7 the standardized fourth and sixth moments are presented. Two significant features can be pointed out. First, the asymptotic values of these moments relax to a constant value that is independent of the initial scalar length scale. However, the manner in which the curves approach the final value is seen to depend on the initial state of the scalar field. At early times, the simulations initialized with the smaller scalar length scales show a rapid increase in their higher-order moments before relaxing to their final state. In the case presented here, the final values of the fourth and sixth moment are somewhat less than the corresponding Gaussian values of 3 and 15. It was indicated both by Eswaran and Pope[4] and McMurtry and Givi[3] in their DNS studies that the pdf apparently tended toward Gaussian in the limit as the scalar rms became small. However, more recent analytical work[12] and simulations[13] suggest that non-Gaussian behavior may persist throughout the mixing process. Further discussion of this matter is deferred to Sec. IV B 1.

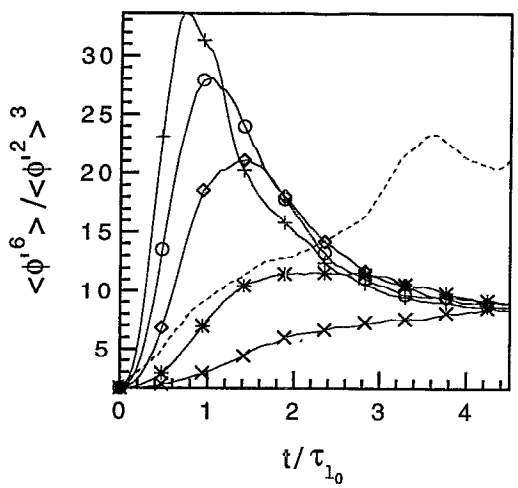

FIG. 7. Evolution of the superskewness (normalized sixth moment) from the linear eddy model for the same cases as Fig. 6. Eswaran and Pope DNS results for $k_s/k_0=4$ are indicated by dashed line.

The dependence of ϵ_ϕ on ϕ can be examined by computing the correlation function $\rho \equiv \langle \phi^2 \epsilon_\phi \rangle / (\langle \phi^2 \rangle \langle \epsilon_\phi \rangle) - 1$. Comparison of this quantity with the DNS results is shown in Fig. 8. Quantitative and qualitative differences are apparent. For the conditions considered ($Sc_S=0.7$, $Re_S=90$), the model predicts that ρ converges to a nonzero value, while DNS indicates eventual convergence to a different value. The linear eddy result indicates a lasting dependence of ϵ_ϕ on ϕ, consistent with the persistence of non-Gaussian behavior[11] evident in Figs. 6 and 7. This quantity also displays a Sc_S dependence as shown in Sec. IV B 1.

As mentioned in Sec. III C, the quantitative discrepancy between the linear-eddy results and the DNS results shown in Figs. 6–8 may reflect the use of high-Re scalings in a moderate-Re application. High-Re scaling may result in a larger contribution of the small scales to the mixing process than occurs in a moderate-Re DNS. This is consistent with the differences observed in the decay of the scalar rms at smaller initial scalar length scales and in the initial development of the scalar dissipation for all cases. On the other hand, the differences between the linear eddy results and the DNS may reflect a fundamental limitation of the linear eddy model with respect to its representation of mixing kinematics. This issue can be resolved on the basis of DNS and/or laboratory experiments at higher Re.

In general, the linear eddy model is found to accurately represent important features of the turbulent mixing process. The agreement is particularly remarkable considering

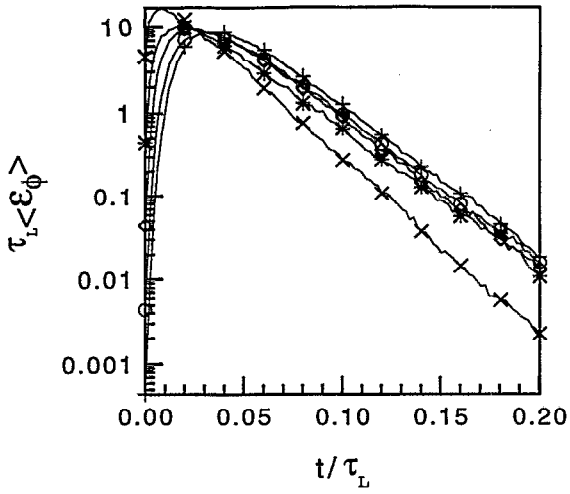

FIG. 9. Evolution of the scalar dissipation for $Re_S=90$, $k_s/k_0=1$ at different values of Sc_S as computed from linear eddy model. (×, $Sc_S=0.1$), (*, $Sc_S=1.0$), (◇, $Sc_S=10$), (○, $Sc_S=100$), and (+, $Sc_S=1000$).

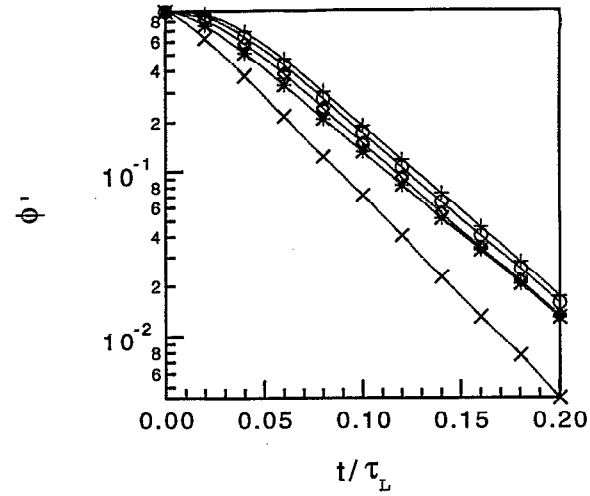

FIG. 10. Evolution of the scalar field rms for the same cases as Fig. 9.

that the scaling laws upon which the model is built are based on high-Re turbulent flows, and the DNS results have been obtained for relatively moderate-Re flows.

B. Reynolds and Schmidt number sensitivities

Owing to the severe computational requirements of DNS, previous DNS of turbulent mixing has necessarily been limited in the range of Re and Sc that could be treated. The effects of Re and Sc on the overall mixing process have not as yet been quantified. However, with the computationally economical one-dimensional formulation of the linear eddy model, a much wider range of length scales can be treated, allowing parametric Re and Sc studies. In the simulation results that follow, results are parametrized by Re_S and Sc_S, whose relation to the physical quantities Re and Sc is discussed in Sec. III. The initial scalar fields for all simulations that follow were initialized with a value of $k_s/k_0=1$, unless otherwise noted.

1. Schmidt number dependence

The linear eddy model was used to perform simulations spanning a range of $Sc_S=0.1$–1000 for $Re_S=90$. The moderate-Re case was selected for Sc_S comparisons, as resolution requirements become severe when resolving the Batchelor scale for high Schmidt number flows, even in one spatial dimension. Sc_S sensitivities are shown in Figs. 9–12.

Figure 9 indicates that the initial growth rate of the dissipation at a fixed Reynolds number is independent of Schmidt number. This Sc independence persists until the scalar length scale is reduced to the Batchelor scale, where molecular diffusion effectively smooths out scalar gradients. The time at which the dissipation reaches its maximum value (i.e., the time to reach the Batchelor scale) is seen to increase with increasing Sc. This is quantified in the following paragraph. Subsequently, the magnitude of the dissipation, when scaled by the large eddy turnover time, τ_L, is independent of Sc for $Sc_S \geqslant 1$. This is consistent with $\epsilon_\phi \sim \phi'^2/\tau_L$, where ϕ' is an order unity quantity.

The time at which the scalar dissipation peaks is also consistent with conventional scaling analysis. The maximum dissipation will occur when the scalar length scale is reduced to the Batchelor scale, l_B. For $Sc>1$, this time, $\hat{t}$ can be estimated in two steps: $\hat{t}=t_1+t_2$, where t_1 is the time to reach the Kolmogorov scale, and t_2 is the additional time to reach the Batchelor scale. To estimate t_1, consider the size evolution $l(t)$ of a scalar blob initially of size $l(0)=L$. Based on dimensional considerations applicable to the inertial-range cascade,[20] that evolution is governed by $dl/dt=-l/t_l$, where the characteristic eddy time t_l scales according to $t_l \sim (l/L)^{2/3}\tau_L$. Integrating from the integral scale L to η gives $t_1/\tau_L=[1-(\eta/L)^{2/3}]=1-\mathrm{Re}^{-1/2}$. (Numerical coefficients are suppressed here, but are restored shortly.) This demonstrates the Re sensitivity (van-

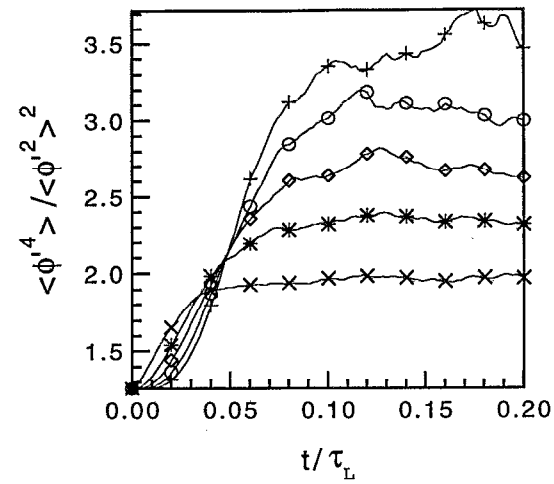

FIG. 11. Evolution of kurtosis of the scalar field for the same cases as Fig. 9.

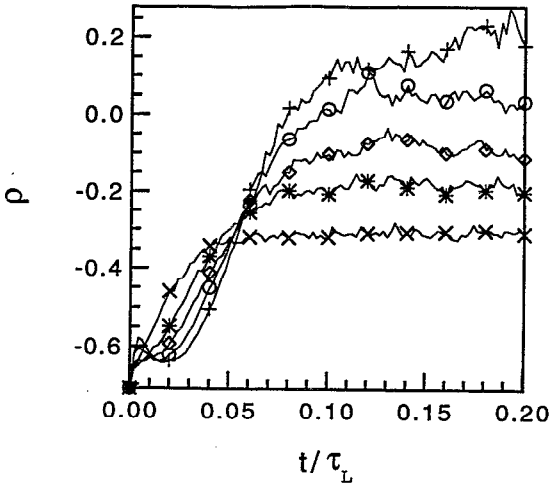

FIG. 12. Evolution of the scalar variance-dissipation correlation function for the same cases as Fig. 9.

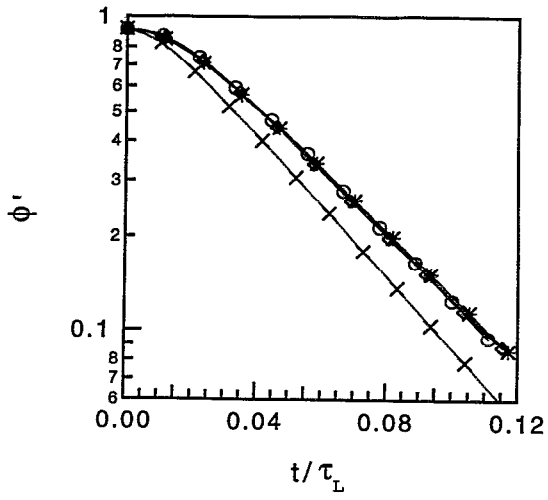

FIG. 13. Evolution of the scalar rms ϕ' for $Sc_S=1$ at different values of Re_S. (×, $Re_S=10$), (*, $Re_S=100$), (◇, $Re_S=1000$), and (+, $Re_S=10\,000$).

ishing at high Re) of the time (in units of τ_L) for a scalar blob to traverse the inertial range.

Further length scale reduction to the Batchelor scale l_B occurs at an exponential rate. For $Sc \gg 1$, $l_B=\eta \exp(-t_2/\tau_K)$, where τ_K is the Kolmogorov time and $\eta/l_B=A/Sc^{1/2}$, where A is a coefficient. Since $\tau_K=B\,Re^{-1/2}\tau_L$, where B is another coefficient, this gives $t_2/\tau_L=B(\ln A+\frac{1}{2}\ln Sc)Re^{-1/2}$. Combining t_1 and t_2, $\hat{t}$ can be expressed in the general form

$$\hat{t}/\tau_L=c_1+Re^{-1/2}(c_2+c_3 \ln Sc), \tag{3}$$

where the coefficients c_1 and c_3 are positive, but c_2 can be of either sign. This relationship can be interpreted in terms of the model quantities Re_S and Sc_S. The $\ln Sc_S$ dependence on the time of peak dissipation is borne out in Fig. 9.

The decay of the scalar rms (Fig. 10) shows little Sc_S dependence for $Sc_S > 1$. The behavior of the scalar rms is consistent with the scalings presented above and the behavior of the scalar dissipation shown in Fig. 9.

The foregoing results are not surprising, in view of the fact that the underlying scaling properties are, in effect, built into the model, as discussed in Sec. II. They, nevertheless, serve as further verification that the event frequency provides a valid basis for estimating an effective eddy-turnover time, despite the fact that model events representing individual eddies are, strictly speaking, instantaneous. Furthermore, the plotted results serve as a concrete manifestation, in the present context, of well-established scaling principles, much as Kosály[21] showed that features of the rms decay curves are subtle manifestations of those principles.

The higher-order moments display an interesting Sc_S dependence (Fig. 11), which is also reflected in the scalar variance-scalar dissipation correlation function (Fig. 12). In general, the low-Sc simulations give values of the kurtosis and superskewness well below Gaussian values. As Sc_S is increased, the values of both the kurtosis and superskewness increases. This trend is apparent over the Sc_S range studied. For Sc_S of order unity, the moments are below their Gaussian values, while for high Sc_S, the final values of the higher-order moments are near the Gaussian values.

The occurrence of non-Gaussian pdf's can be understood as follows. If fine-scale mixing is fast relative to large-scale stirring, small regions will become well mixed while large-scale variations of ϕ are still present. Each small, mixed region converges to a Gaussian distribution whose mean corresponds to the local mean value of ϕ, which generally differs from the global mean value $\phi=0$. Therefore the core of the spatially averaged pdf consists of a superposition of Gaussians with different mean values, yielding a distribution that may be longer tailed or shorter tailed than Gaussian. Since this mechanism is predicated on the relative efficacy of the fine-scale mixing, it implies that the linear eddy results reflect a larger contribution of the small scales to the mixing process than occurs in the DNS. In this regard, the results for the higher moments are consistent with the results for pdf evolution, discussed in Sec. IV A.

2. Reynolds number effects

The decay rate of the scalar rms is shown in Fig. 13 for $Re_S=10$–$10\,000$ and $Sc_S=1$. With time nondimensionalized for each case by its large eddy turnover time, τ_L, all curves at or above $Re_S=100$ collapse. This indicates that, in terms of the model parameters, high Reynolds number similarity is obtained at $Re_S=100$. For the case of $Sc_S=1$ considered here, the scalar dissipation decreases rapidly at the Kolmogorov scale. The time to reach this scale, as discussed in Sec. IV B 1, is $t_1=\tau_L(1-Re^{-1/2})$. This is consistent with the small Re_S effect, which vanishes at high Re_S, seen in the model results.

The effects of Re_S on the scalar dissipation evolution are shown in Fig. 14. The maximum value of the scalar dissipation is independent of Re_S when scaled with τ_L.

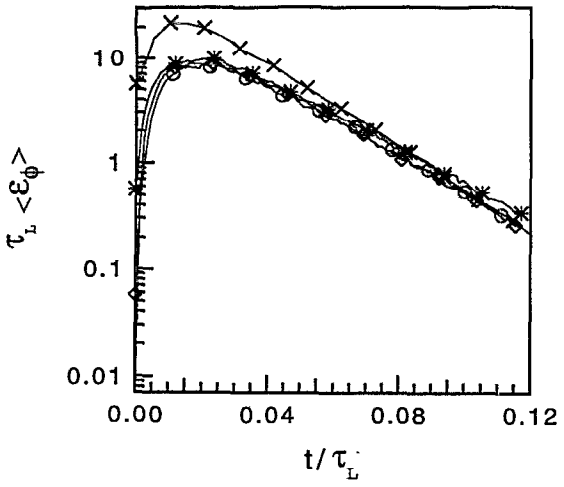

FIG. 14. Evolution of the scalar dissipation for $Sc_S=1$, $k_s/k_0=1$ for the same cases as in Fig. 13.

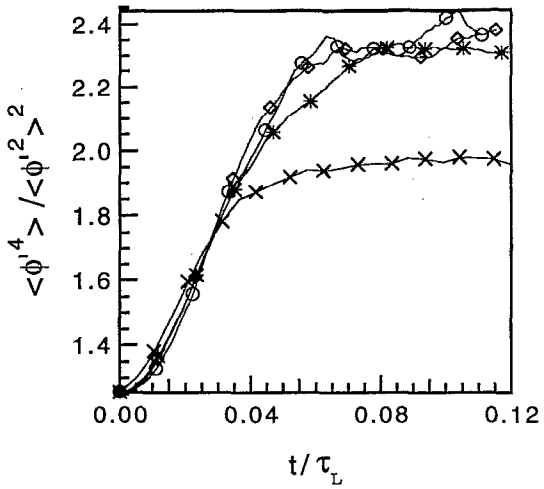

FIG. 16. Evolution of the kurtosis of the scalar field for the same cases as Fig. 13.

This agrees with the scaling analysis outlined in Sec. IV B 1. Furthermore, the time at which the scalar dissipation peaks can also be interpreted by the scaling analysis summarized by Eq. (3). First, Eq. (3) indicates there will be a unique value of Sc_S at which the Re_S dependence will vanish. The lack of Re_S sensitivity in Fig. 14 indicates that $Sc_S=1$ is near this value. Second, as Sc_S is increased above this value, the Re_S sensitivity should increase. Computed results for $Sc_S=10$ exhibit this trend (Fig. 15).

The evolution of the scalar pdf, as described by the higher-order moments, does not show a strong Re dependence beyond $Re_S=100$ (Fig. 16). This and the foregoing results indicate that Re effects may be sufficiently well characterized by studying a limited range of Re. However, a complete understanding of Sc effects may require wider-ranging study and improved analytical methods.

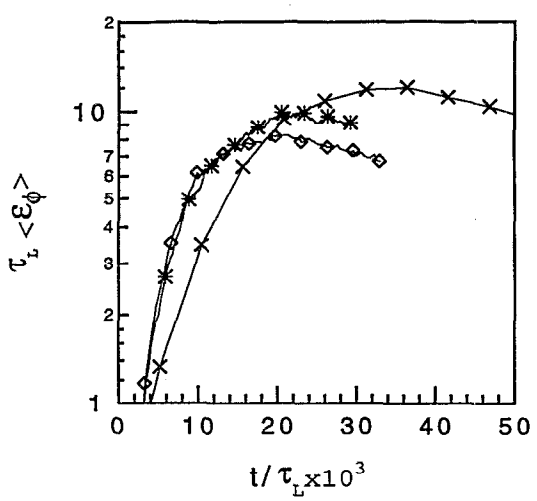

FIG. 15. Initial development of the scalar dissipation for $Sc_S=10$, $k_s/k_0=1$ at different values of Re_S. (×, $Re_S=10$), (*, $Re_S=100$), and (◇, $Re_S=1000$).

V. CONCLUSIONS

Various aspects of the time evolution of a passive scalar field in steady homogeneous turbulence have been addressed here using the linear eddy modeling approach. The model formulation in one spatial dimension incorporates the mechanisms needed to represent the dependences of mixing properties on Re and Sc.

Detailed comparisons with moderate-Re DNS for Sc of order unity indicate that the model captures the dependence of scalar rms and scalar dissipation evolution on the initial scalar length scale. Principal features of scalar pdf evolution are reproduced. Quantitative discrepancies with respect to structural properties of the mixing field may reflect inherent limitations of the model, or may reflect the fact that moderate-Re DNS does not fully conform to the inertial-range scaling laws built into the model. DNS or laboratory experiments at higher Re could resolve this ambiguity.

Parametric sensitivities were investigated based on Sc and Re variations over several orders of magnitude. The parametric study demonstrates that the computed transient evolution of the scalar field obeys the appropriate high-Re scaling properties and exhibits finite-Re departures from scaling that are consistent with the classical picture of mixing kinematics in the inertial and viscous subranges. These observations complement a previous study,[15] which demonstrated conformance of the model to that picture in the context of steady-state homogeneous mixing. Collectively, these results highlight the common origin of the steady-state spectral scalings and the scalings governing a transient mixing field in steady homogeneous turbulence. Moreover, these results demonstrate that a comprehensive picture of turbulent mixing kinematics can be embodied in a mathematical formulation of reduced spatial dimensionality, provided that the underlying physical processes and their associated length and time scales are explicitly represented.

The parametric study provided new insights into the

mechanisms underlying the evolution of the scalar pdf. Qualitative as well as quantitative features of this evolution were found to be sensitive to Sc, consistent with a simple mechanistic picture. This picture indicates that the shape of the pdf in the final stages of mixing depends on mechanistic details not represented in other models that have been applied to the question of pdf evolution. Improved analytical methods are needed in order to quantify the impact of these mechanisms, and to determine why models lacking the mechanisms governing Sc sensitivity agree well with DNS results for a particular value of Sc. Tests of the predicted sensitivities, by means of high-Sc laboratory experiments or DNS, would serve both to check the predictions and to stimulate further analytical study.

ACKNOWLEDGMENTS

This work was supported in part by the Office of Naval Research under Grant No. N0001491J1175; the Division of Engineering and Geosciences, Office of Basic Energy Sciences, U.S. Department of Energy; and the Advanced Combustion Engineering Research Center. Funds for the research center are received from the National Science Foundation, the state of Utah, 26 industrial participants, and the U.S. Department of Energy.

[1]R. L. Curl, "Dispersed phase mixing: I. Theory and effects in simple reactors," AIChE J. **9**, 175 (1963).
[2]D. Dopazo and E. E. O'Brien, "Statistical treatment of nonisothermal chemical reactions in turbulence," Combust. Sci. Technol. **13**, 99 (1978).
[3]P. A. McMurtry and P. Givi, "Direct numerical simulations of mixing and reaction in a nonpremixed homogeneous turbulent flow," Combust. Flame **77**, 171 (1989).
[4]V. Eswaran and S. B. Pope, "Direct numerical simulations of the turbulent mixing of a passive scalar," Phys. Fluids **31**, 506 (1988).
[5]Z. Warhaft, "The interference of thermal fields from line sources in grid turbulence," J. Fluid Mech. **144**, 363 (1984).
[6]W. E. Mell, G. Kosály, and J. J. Riley, "The length scale dependence of scalar mixing," Phys. Fluids A **3**, 2474 (1991).
[7]J. Janicka, W. Kolbe, and W. Kollmann, "Closure of the transport equation for the probability density function of turbulent scalar fields," J. Non-Equilib. Thermodyn. **4**, 47 (1979).
[8]L. Valiño and C. Dopazo, "A bimodal Langevin model for turbulent mixing," Phys. Fluids A **3**, 3034 (1991).
[9]H. Chen, S. Chen, and R. H. Kraichnan, "Probability distribution of a stochastically advected scalar field," Phys. Rev. Lett. **63**, 2657 (1989).
[10]S. B. Pope, "Mapping closure for turbulent mixing and reaction," in *Studies in Turbulence: In Recognition of Contributions by John Lumley*, edited by T. B. Gatski, S. Sarkar, and C. G. Speziale (Springer-Verlag, Berlin, 1991), p. 255.
[11]E. E. O'Brien and T.-L. Jiang, "The conditional dissipation rate of an initially binary scalar in homogeneous turbulence," Phys. Fluids A **3**, 3121 (1991).
[12]F. Gao, "Mapping closure and non-Gaussianity of the scalar probability density functions in isotropic turbulence," Phys. Fluids A **3**, 2438 (1991).
[13]F. Gao, Y. Kimura, and R. H. Kraichnan, "Non-Gaussianity of a scalar probability density function (PDF) induced by random advection," Bull. Am. Phys. Soc. **36**, 2662 (1991).
[14]A. R. Kerstein, "Linear eddy model of turbulent scalar transport and mixing," Combust. Sci. Technol. **60**, 391 (1988).
[15]A. R. Kerstein, "Linear eddy modeling of turbulent transport. Part 6. Microstructure of diffusive scalar mixing fields," J. Fluid Mech. **231**, 361 (1991).
[16]A. R. Kerstein, "Linear eddy modeling of turbulent transport. Part 7. Finite-rate chemistry and multi-stream mixing," J. Fluid Mech. **240**, 289 (1992).
[17]A. R. Kerstein, "Linear eddy modeling of turbulent transport II: Application to shear layer mixing," Combust. Flame **75**, 397 (1989).
[18]A. R. Kerstein, "Linear eddy modeling of turbulent transport. Part 3. Mixing and differential molecular diffusion in jets," J. Fluid Mech. **216**, 411 (1990).
[19]J. E. Broadwell and M. G. Mungal, "Large-scale structure and molecular mixing," Phys. Fluids A **3**, 1193 (1991).
[20]H. Tennekes and J. L. Lumley, *A First Course In Turbulence* (MIT Press, Cambridge, MA, 1974), pp. 258–259.
[21]G. Kosály, "Scalar mixing in homogeneous turbulence," Phys. Fluids A **1**, 758 (1989).